BIOCHEMISTRY
including biophysical chemistry & molecular biology

Article

pubs.acs.org/biochemistry

Modular Unfolding and Dissociation of the Human Respiratory Syncytial Virus Phosphoprotein P and Its Interaction with the M_{2-1} Antiterminator: A Singular Tetramer−Tetramer Interface Arrangement

Sebastián A. Esperante,[†] Gastón Paris,[‡] and Gonzalo de Prat-Gay*[,†]

[†]Protein Structure-Function and Engineering Laboratory and [‡]Molecular Immunology and Microbiology Laboratory, Fundación Instituto Leloir and IIBA-Conicet, Patricias Argentinas 435, (1405) Buenos Aires, Argentina

ABSTRACT: *Paramyxoviruses* share the essential RNA polymerase complex components, namely, the polymerase (L), phosphoprotein (P), and nucleoprotein (N). Human respiratory syncytial virus (RSV) P is the smallest polypeptide among the family, sharing a coiled coil tetramerization domain, which disruption renders the virus inactive. We show that unfolding of P displays a first transition with low cooperativity but substantial loss of α-helix content and accessibility to hydrophobic sites, indicative of loose chain packing and fluctuating tertiary structure, typical of molten globules. The lack of unfolding baseline indicates a native state in conformational exchange and metastable at 20 °C. The second transition starts from a true intermediate state, with only the tetramerization domain remaining folded. The tetramerization domain undergoes a two-state dissociation/unfolding reaction (37.3 kcal mol^{-1}). The M_{2-1} transcription antiterminator, unique to RSV and *Metapneumovirus*, forms a nonglobular P:M_{2-1} complex with a 1:1 stoichiometry and a K_D of 8.1 nM determined by fluorescence anisotropy, far from the strikingly coincident dissociation range of P and M_{2-1} tetramers (10^{-28} M^3). The M_{2-1} binding region has been previously mapped to the N-terminal module of P, strongly suggesting the latter as the metastable molten globule domain. Folding, oligomerization, and assembly events between proteins and with RNA are coupled in the RNA polymerase complex. Quantitative assessment of the hierarchy of these interactions and their mechanisms contribute to the general understanding of RNA replication and transcription in *Paramyxoviruses*. In particular, the unique P−M_{2-1} interface present in RSV provides a valuable antiviral target for this worldwide spread human pathogen.

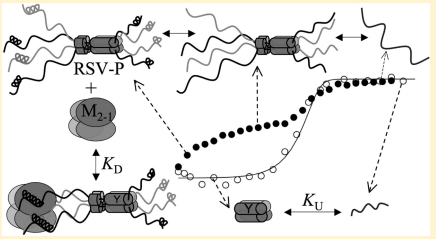

The *Paramyxoviridae* family includes some of the ubiquitous and disease-causing viral pathogens in humans and animals and belongs to the order *Mononegavirales* (the nonsegmented negative-strand RNA viruses). It comprises two subfamilies: *Paramyxovirinae,* which includes the human parainfluenza viruses type 1−4, measles, mumps, and others, and *Pneumovirinae,* which is represented by the respiratory syncytial virus (RSV).[1] Human respiratory syncytial virus (HRSV) infects almost everyone worldwide and can cause severe respiratory illness in particular during infancy, early childhood, elderly people, and immunosuppressed patients. It is the leading cause of pediatric hospitalization for lower tract respiratory disease.[2] Over 125 000 hospitalizations related to RSV and 1.5 million outpatient visits occur among infants in the United States.[3,4] A systematic review from 2005 indicated 34 million new episodes of severe low respiratory tract infections worldwide, with over 20 000 fatal cases, where 99% of them occur in developing countries.[5]

The RSV genome is composed of a single-stranded nonsegmented negative-sense RNA of ∼15 kb in length which is encapsidated by the nucleocapsid (N) protein. The resulting ribonucleoprotein complex (N-RNA) is the template for transcription and replication of the viral genome by the RNA-dependent RNA polymerase complex which comprises the large polymerase protein L, the phosphoprotein P, and the antiterminator factor M_{2-1}.[2] The M2 gene of RSV encodes two different proteins: M_{2-1}, which acts as a transcriptional antiterminator and processivity factor,[6,7] and M_{2-2}, which is involved in the regulation of viral RNA transcription and replication.[8] Aside from the M_2 gene and the nonstructural interferon antagonists, NS1 and NS2, unique to *Pneumovirinae* (*Metapneumovirus* and RSV), the rest of the proteins related to attachment, fusion, matrix, and polymerase complex are present throughout the *Mononegavirales* order, which include many health-threatening pathogens.[9]

The P protein is an essential cofactor of the viral polymerase and plays a central role in viral transcription and replication through its multiple interaction partners within the polymerase complex. P protein was shown to interact with N-RNA,[10−12] the large polymerase L,[13] and M_{2-1}.[14,15] In RSV, the M_{2-1} protein increases the processivity of the viral RNA polymerase by preventing premature termination during transcription and also by enhancing the ability of the polymerase to read through transcription termination signals.[6,16] During viral genome transcription and replication, P is believed to position L onto

Received: June 8, 2012
Revised: August 13, 2012

   dx.doi.org/10.1021/bi300765c | *Biochemistry* XXXX, XXX, XXX−XXX

the RNA−N template and assist the translocation of the polymerase complex along the helical nucleocapsid, a common mechanism shared by members of the *Paramyxoviridae* family. Further, by analogy to members of the *Paramyxovirinae* and *Rhabdoviridae* families, RSV P is also believed to act as a chaperone for N maintaining the newly synthesized N polypeptide in a soluble form (N^0). The P−N^0 complex is the substrate for the encapsidation of nascent RNA.[2]

The RSV P protein (241 amino acids) is the smallest among its *Paramyxovirinae* counterparts. However, RSV P seems to have the minimal structural elements required for the conserved P function. *Paramyxovirus* P proteins display a modular structure with three essential domains: the N^0 binding the oligomerization domain that includes the L binding domain and the N-RNA binding domain.[17,18] There is no sequence similarity between Ps of the *Paramyxovirinae* and *Pneumovirinae* subfamilies, but the oligomerization domain, by either actual structures or modeling, comprises mostly α-helices.[17,19]

Cellular casein kinase II phosphorylates RSV P at several serine residues, mainly at the C-terminal Ser-232 with a low phosphorylation turnover[20,21] and also at other phosphorylation sites with intermediate turnover located at the tetramerization domain, such as Ser-116, -117, and -119.[22−24] The effect of phosphorylation at the different sites remains to be clarified as it is dispensable for genome replication.[25] However, recent evidence indicates that P phosphorylation is involved in several key functions within the virus life cycle.[24,26,27]

RSV P was initially proposed to be homotetrameric by size exclusion chromatography (SEC) and chemical cross-linking[28−30] and was later confirmed by sedimentation equilibrium.[31] P elutes from a SEC column with a much higher apparent molecular weight (~500 kDa) than that expected for a globular homotetramer with the same molecular weight (~109 kDa) as a consequence of its elongated shape.[30,31] This anomalous elution from SEC has been reported for other *Paramyxovirus* Ps.[32,33] The oligomerization domain of RSV P has been mapped to the central part of the molecule (amino acids 120−150) using deletion mutants,[11] and an oligomeric trypsin-resistant fragment (fragment X, residues 104−163) was identified.[30] A similar trypsin-resistant fragment from the C-terminal half of Sendai virus (SeV) was shown to form homotetramer in solution and adopted an elongated shape.[32] The high-resolution atomic structure of SeV P oligomerization domain revealed a homotetrameric coiled-coil with each monomer composed of three short N-terminal helices and a very long C-terminal helix. The tetramer consists of a four-helix bundle stabilized by a cluster of hydrophobic residues.[19] Thus, RSV P is predicted to contain a coiled-coil domain spanning residues 130−155,[11,30] and the three-dimensional model of the oligomerization domain was built based on the atomic structure available from Sev.[31] This coiled-coil structure overlaps with the L polymerase-binding domain and is also present in the oligomerization domain of rinderpest virus.[33] Interestingly, oligomeric α-helical-rich tetramers proteins with an elongated shape are also present in distant viruses such as the protein gp11, which is the scaffolding/procapsid assembly protein of bacteriophage SPP1.[34]

Bioinformatic analysis of the P protein from *Pneumovirus* predicted a coiled-coil region (residues 125−146) and the existence of two intrinsically disordered regions (1−99 and 201−241) flanking a central structured coiled-coil tetramerization domain (100−200). The disordered or flexible regions are highly sensitive to proteolysis in vitro and alternate with structured domains or modules, a common feature in viruses from the *Paramyxoviridae* and *Rhabdoviridae* families. A modular organization of Ps consisting of long disordered regions alternating with structured domains has been proposed.[17,35]

In this work, we investigated the unfolding of RSV P and its tetramerization domain, using a biochemical and biophysical approach. We characterized a metastable molten globule-like domain in the native protein, which unfolds to a stable tetrameric intermediate, which undergoes a concomitant unfolding and dissociation. In order to gain insight into the biochemical implications of P, we investigated its interaction with the transcription antiterminator RSV M_{2-1}, unique to *Pneumovirinae*. We obtained quantitative data that are discussed in light of interaction hierarchy among tetramerization and binding and the relevance to the RNA polymerase complex.

EXPERIMENTAL PROCEDURES

Expression and Purification of the HRSV P Protein. The human RSV strain A P sequence was cloned into the BamH I/EcoR I sites of the pRSETA vector (Invitrogen) as an N-terminal 6X His-tagged fusion protein, and the resulting plasmid was sequenced and transformed in *E. coli* BL21 (DE3)pLys for expression. A single colony was grown in 0.5 L of TB medium suplemented with 0.3% glucose at 37 °C containing 100 μg/mL of ampicillin and 35 μg/mL of chloramphenicol. Twelve hours after inoculation 0.3 mM IPTG was added to the culture for induction, and cells were harvested by centrifugation 3 h later. The cell pellet was resuspended in 20 mL of buffer 100 mM Tris-HCl (pH 8.0), 0.6 M NaCl, 5 mM 2-mercaptoethanol, and 1 mM EDTA, lysed by sonication, and centrifuged at 15000*g* for 20 min at 4 °C. The resulting supernatant was precipitated adding solid ammonium sulfate to 40% saturation. The precipitated protein was collected by centrifugation, resuspended, and dialyzed against 50 mM Tris-HCl (pH 8.0), 0.2 M NaCl. After dialysis, the protein sample was incubated 15 min at 75 °C, placed on ice for 5 min, and centrifuged at 16000*g* for 20 min at 4 °C. The resulting soluble fraction was treated with 1 mg of Ribonuclease A (Sigma) and incubated for 4 h at 37 °C. The sample was concentrated using amicon centrifugal filter units (Millipore) and subjected to a size exclusion chromatography on a Superdex 200 gel filtration column (GE Healthcare) in 20 mM Tris-HCl (pH 8.0), 0.2 M NaCl. Protein eluted from this column was >95% pure and was concentrated to 100−150 μM using centrifugal devices, dialyzed against 20 mM sodium phosphate (pH 7.4), 0.05 M NaCl, and stored at −80 °C. The 6X His-tag of the purified P fusion protein was cleaved with thrombin 0.33% (w/w), 2.5 mM $CaCl_2$ for 2 h at 37 °C, and the reaction was stopped by adding 2.0 mM of PMSF. The unfused P protein was purified by SEC (Superdex 200) and concentrated as previously described.

Protein concentration was determined spectrophotometrically using a molar extinction coefficient of ε_{280} 7450 M^{-1} cm^{-1} for 6X His-tagged P and ε_{280} 5960 M^{-1} cm^{-1} for unfused P, calculated using the Expasy ProtParam tool. The protein concentration is expressed as monomer concentration.

Trypsin Digestion of P and Purification of Protease-Resistant Fragment Y. Purified 6X His-tagged P was digested with trypsin from bovine pancreas (Sigma-Aldrich) in 100 mM Tris-HCl (pH 7.5), 50 mM NaCl for 2 h at 37 °C at a ratio 100:1 (protein:trypsin w/w). The reaction was stopped adding 1 mM phenylmethylsulfonyl fluoride (PMSF). The digestion

dx.doi.org/10.1021/bi300765c | *Biochemistry* XXXX, XXX, XXX−XXX

products were separated in an SEC column (Superdex 75) in 20 mM Tris-HCl (pH 8.0), 0.2 M NaCl. The elution peaks were analyzed by SDS-PAGE stained with Coomassie Blue. The trypsin used contains some contaminating chymotripsin; thus, the peptide obtained was fragment Y as previously described,[31] and the molecular weight was determined by mass spectrometry. The peptide was concentrated with centrifugal devices to ~500−600 μM, and the concentration was measured spectrophotometrically using a molar extinction coefficient of ε_{280} 1490 M^{-1} cm^{-1} calculated using the Expasy ProtParam tool.

Size Exclusion Chromatography. Size exclusion chromatographies were carried out on a Superdex 75 HR 10/30 (24 mL), a Superdex 200 HR 10/30 (24 mL), or a Superose 6 HR 10/30 (24 mL) columns (GE Healthcare). The S200 column was calibrated with the following standard globular proteins: ferritin (440 kDa), catalase (232 kDa), BSA (67 kDa), ovalbumin (43 kDa), chymotrypsinogen A (25 kDa). The Superose 6 column was calibrated with Thyroglobulin (669 kDa), ferritin, BSA, and chymotrypsinogen A. The S75 column was calibrated with BSA, chymotrypsinogen A, and ribonuclease A (13.7 kDa) from a gel calibration kit (Pharmacia Biotech, Uppsala, Sweden). The void volume (V_0) and total volume (V_t) were determined by loading Blue Dextran and acetone, respectively. The buffers used in the runs are indicated in each case.

Light Scattering. The average molecular weight of the proteins were determined by static light scattering (SLS) using a Precision Detector PD2010 light scattering instrument connected in tandem to a high-performance liquid chromatography system and an LKB 2142 differential refractometer. The 90° light scattering and refractive index signals of the eluting material were recorded on a PC computer and analyzed with the Discovery32 software supplied by Precision Detectors. The protein concentration used in each SEC run to determine the average molecular weight were 40 μM of M_{2-1}, 30 μM of P, and 40 μM:30 μM of the M_{2-1}:P complex (excess of M_{2-1} to ensure that the complex was composed only by P and M_{2-1}).

The determination of the hydrodynamic size distribution of P by dinamic light scattering (DLS) was performed on a Zetasizer Nano S DLS device from Malvern Instruments (Malvern). The solutions were centrifuged at 14000*g* for 10 min at 4 °C and filtered with Ultrafree-MC microcentrifuge filters (0.22 μm, Millipore) before measurements were taken.

Chemical Denaturation Experiments. The stock solutions used contained either 7.5 M Gdm.Cl or 10 M urea. The buffer used for unfolding experiments was 20 mM sodium phosphate (pH 7.4), 0.1 M NaCl, and the corresponding Gdm.Cl or urea concentration. The protein samples (P or fragment Y) were incubated with the chemical denaturant for a minimum of 16 h prior to measurement. The protein concentration used in each case is indicated in the figure legend.

Circular Dichroism (CD) and Fluorescence Spectroscopy. Far-UV CD measurements were conducted on a Jasco J-810 spectropolarimeter using a Peltier temperature-controlled sample. Spectra between 200 and 260 nm were recorded at a rate of 200 nm/min, a response time of 2 s, and a bandwidth of 2 nm. All spectra were an average of at least four scans. Spectra of P at 10 and 1 μM were taken on 0.1 and 0.5 cm path length cells, respectively. The path length used for obtaining spectra of fragment Y were 0.1 cm (25 μM of Y), 0.2 cm (12 μM of Y), and 0.5 cm (5.0 and 2.5 μM of Y). The ellipticity at 260 nm was subtracted from the other ellipticities as a baseline value. The results are expressed as degrees per square centimeter per dmol.

Fluorescence emission spectra were recorded on a Jasco FP-6500 spectrofluorometer.

The fluorescence emission spectra for ANS binding were carried out with an excitation wavelength at 370 nm and 5 nm band-pass, and the ANS concentration used was 100 μM. All data shown are an average of at least five spectra and were corrected subtracting the buffer background at the appropriate Gdm.Cl or urea concentration.

Glutaraldehyde Cross-Linking. The P protein solutions at 10 or 1 μM were incubated for 16 h at a given Gdm.Cl concentration in 20 mM sodium phosphate (pH 7.4), 0.1 M NaCl. The samples were then treated with 0.1% glutaraldehyde and incubated for 2 min at room temperature, and the reactions were stopped by adding 100 mM Tris-HCl (pH 7.5) and 50 mM $NaBH_4$. The samples were diluted 10 times with 50 mM sodium phosphate (pH 7.4), 0.1 M NaCl, and precipitated on ice with 10% TCA (trichloroacetic acid) for 30 min. The samples were then centrifuged at 14000*g* for 10 min at 4 °C, and the pellet was washed twice with ice-cold acetone and resuspended in 20 μL of SDS sample buffer. Finally, the samples were boiled and loaded onto a 12.5% SDS−polyacrylamide gel and stained with Coomassie Blue.

FITC Labeling of P and Fluorescence Anisotropy Titrations. In the labeling reaction 3−4 mg/mL of P was labeled with 0.4−0.6 mg/mL of FITC (~10-fold molar excess of FITC) in 100 mM sodium carbonate buffer (pH 9.0) for 2 h at room temperature in the dark. The reaction was stopped by adding 100 mM Tris-HCl pH 8.0 and was incubated for 1 h at room temperature. The labeling reagents were separated by a desalting column (PD-10; GE Healthcare, Uppsala, Sweden), followed by a Superdex 200 SEC. The purity of all preparations was evaluated using MALDI-TOF spectroscopy, and the labeled P protein was quantified by a Bradford colorimetric assay using bovine serum albumin (BSA) as standard. The FITC concentration was determined at pH 7.4 by measuring the absorbance at 494 nm using a molar extinction coefficient of 75 000 M^{-1} cm^{-1}.[36] Fluorescence anisotropy titration measurements were conducted using an Aminco-Bowman Series 2 spectrofluorimeter. The fluorescein-labeled protein was diluted to the desired concentration. The assay buffer consisted of 20 mM sodium phosphate (pH 7.4), 0.3 M NaCl, 1 mM DTT, and 10 μM SO_4Mg_2. The M_{2-1} protein was obtained and quantified as previously described[37] and was diluted appropriately in stepwise dilutions. Increasing amounts of M_{2-1} were added to a cuvette containing a fixed amount of FITC labeled P and were incubated at least for 2 min to ensure that measurements were taken at steady state at 20 °C. The total volume reached less than 10% in each assay, and thus, the concentration of FITC-P protein can be assumed to have remained constant. Parallel and perpendicular emission components were measured in L-format by excitation at 495 nm and emission at 520 nm. Anisotropy was measured five times at each titration point with an integration time of 2 s, and the resulting anisotropy values were averaged.

The dissociation constant (K_D) of the complex was calculated by fitting the plot of observed fluorescence anisotropy (r) change of FITC labeled P versus added M_{2-1} to the following equation assuming a 1:1 stoichiometry.[38]

dx.doi.org/10.1021/bi300765c | *Biochemistry* XXXX, XXX, XXX−XXX

$$r = r_{free} + \frac{\Delta r_{int}}{2}\{(\chi + [P] + K_D) - [(\chi + [P] + K_D)^2 - 4[P]\chi]^{0.5}\} \quad (1)$$

where χ is the variable total concentration of M_{2-1}, [P] is the total concentration of FITC-P which is held constant, Δr_{int} is the difference in intrinsic fluorescence anisotropy between the free and complexed protein, and r_{free} is the fluorescence anisotropy of P. Data fitting was performed using PROFIT (Quantumsoft, Zurich, Switzerland).

Modeling of Fragment Y Unfolding. We considered a two-state unfolding model in order to estimate the thermodynamic parameters for the transition, a simple tetramer-unfolded monomer equilibrium:

$$N_4 \overset{K_U}{\leftrightarrow} 4U \quad (2)$$

where N_4 is the native tetramer, U is the unfolded monomer, and K_U is the dissociation/unfolding constant for the equilibrium. The equilibrium constant K_U and the fractional populations of native tetramer (f_N) and unfolded monomer (f_U) are defined by

$$K_U = \frac{[U]^4}{[N_4]}; \quad f_N = \frac{4[N_4]}{P_t}; \quad f_U = \frac{[U]}{P_t} \quad (3)$$

where P_t is the total protein concentration. By considering that the sum of the fractional populations f_N and f_U equals 1, the fraction of unfolded monomer (f_U) can be calculated by solving the following quartic equation, as previously shown by Mateu and Fersht.[39]

$$\frac{4P_t^3}{K_U} f_U^4 + f_U - 1 = 0 \quad (4)$$

The relevant real root of this equation gives the solution for f_U, and the fraction of native tetramer (f_N) is

$$f_N = 1 - f_U \quad (5)$$

The molar ellipticity at 222 nm signal was fit to the linear function

$$y = f_N y_N + f_U y_U \quad (6)$$

where y_N and y_U represent the spectroscopic signal of the tetrameric and monomeric unfolded species. The free energy of unfolding was considered to depend linearly on Gdm.Cl concentration and was related to the equilibrium constants K_U.

$$K_U = e^{-(\Delta G^{H_2O} - m[GdmCl])/RT} \quad (7)$$

We performed nonlinear global fitting of the far-UV CD data, obtained from equilibrium unfolding experiments performed at 2.5, 5.0, 12.0, and 25.0 μM fragment Y concentration in order to obtain estimates for the relevant thermodynamic parameters ΔG^{H_2O}, K_U, and m.

RESULTS

Conformational Properties and Stability of P. Since RSV P is at the center of RNA replication and transcription, our initial goal was to investigate its conformational stability and dissociation reaction, using it as a model for Ps from other viruses, in addition to the relevance of its specific interactions in connection with the life cycle of RSV. For this, we expressed and purified human RSV P from bacteria, obtained the proteolysis limit fragment Y (tetramerization domain), and characterized them in detail. The tetrameric nature and elongated shape of P and fragment Y were evaluated by static light scattering (SLS) coupled to size exclusion chromatography (SEC) (Figure 1A). Fragment Y (4.6 kDa) was previously reported to elute as a species that corresponds to a molecular mass of ~129 kDa and behaved as a ~9 kDa polypeptide in SDS-PAGE.[31] With the protein digestion

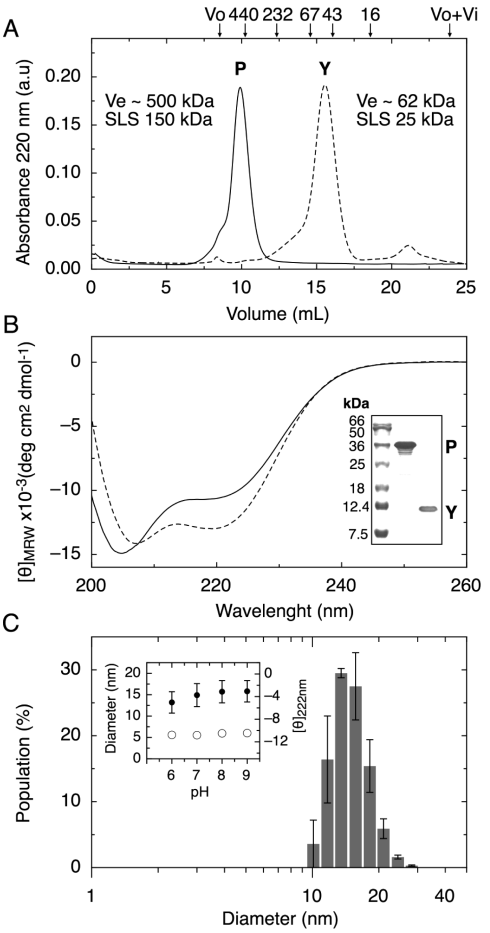

Figure 1. Hydrodynamic properties and secondary structure of RSV-P and fragment Y. (A) Size exclusion chromatographies of purified P and fragment Y in a Superdex 200 column. The upper arrows above the graph denote the positions of void volume (V_0), molecular size standards in kDa, and total volume ($V_0 + V_i$). According to the column calibration, the P and fragment Y peaks correspond to spherical ~500 and 62 kDa species, respectively (indicated as V_e ~ elution volume). The average molecular weight of the peaks, determined by static light scattering, is also indicated (SLS: P 150 kDa and fragment Y 25 kDa). The buffer used was 20 mM sodium phosphate pH 7.4, 0.3 M NaCl. (B) Far-UV CD spectra of purified P (solid line) and fragment Y (dashed line), in 20 mM sodium phosphate pH 7.4, 0.05 M NaCl. Inset: purified recombinant His-tagged P and fragment Y. 18% SDS-PAGE stained with Coomassie Blue. Lane 1, molecular weight marker in kDa. Lane 2, purified His-tagged P. Lane 3, purified fragment Y. (C) Hydrodynamic diameter and secondary structure of P at different pHs. Particle size distribution of 20 μM P at pH 7.0 measured by DLS. Inset: 20 μM of P was incubated in broad range buffer at different pHs (100 mM Tris-HCl, 50 mM MES, 50 mM sodium acetate and 0.1 M NaCl; buffer pHs 6, 7, 8, and 9) for 4 h. The hydrodynamic diameter (●) measured by DLS (left *Y*-axis) and the molar ellipticity at 222 nm (○) measured by CD (right *Y*-axis) as a function of pH is represented. The measurements were taken at 20 °C.

dx.doi.org/10.1021/bi300765c | *Biochemistry* XXXX, XXX, XXX–XXX

protocol we used (see Experimental Procedures), we obtained a major species of fragment Y of 4959.6 Da determined by mass spectrometry, which fits well with a peptide containing three additional residues (Ser-Ala-Arg) in the carboxy terminal region (peptide starting at Ser 119 and ending at Arg 163 with a theoretical mass of 4958.4 Da). We observed that its hydrodynamic behavior corresponds to a globular ~62 kDa species in a Superdex 200 column (Figure 1A) and ~56 kDa species in a Superdex 75 column (not shown). In both cases, an apparent average molecular weight of 25 kDa (20 kDa from sequence) was determined by SLS. In our hands, the Y fragment behaves as a ~12 kDa species in SDS-PAGE (Figure 1B, inset), which is rather anomalous, given its molecular weight of 4.9 kDa from mass spectra. The average molecular weight of His-tagged P from SLS was determined to be 150 kDa (124.4 kDa from sequence), and there appears to be a slight overestimation in both cases, suggesting an artifact caused by its anomalous behavior. The His-tagged P protein eluted in a Superdex 200 column at a position that corresponds to a molecular mass between 450 and 500 kDa (Figure 1A), which is in agreement with a previous report.[30]

Far-UV CD spectra indicated a higher proportion of α-helix in Y (Figure 1B), as expected from sequence homology and structure modeling and from the fact that large disordered regions are absent.[31] A shift of the minimum to 208 nm is indeed an indication of the elimination of disordered nonhelical regions.[30] The secondary structure of P remained unchanged from pH 9.0 to pH 6.0 (Figure 1C, inset), and the protein precipitated below pH 5.8. The hydrodynamic diameter of P was determined to be 14.9 ± 2.6 nm at pH 7.0 by DLS (Figure 1C), corresponding to a 560 kDa globular species,[40] and this value remains unchanged within the same pH range where it remains stable in solution (Figure 1C, inset).

An essential feature to be investigated in a complex/multidomain protein is its conformational stability and the possible equilibria involved, which in turn will dictate interaction with viral and host proteins or RNA. We perturbed its conformational equilibrium using chemical denaturation with Gdm.Cl and urea at 10 μM RSV P concentration and analyzed secondary structure changes by monitoring ellipticity at 222 nm (Figure 2A). The first observation was that the highest concentration of urea was not enough to denature the protein completely, with an almost noncooperative transition and no unfolded state baseline, which made us discard this denaturant as a method of choice. The Gdm.Cl denaturation transition showed at least three states, with a first weak transition with low cooperativity which is over around 2 M denaturant, where the overall cooperative unfolding process is completed after 6 M denaturant (Figure 2A).

The modular mixed globular and putative disordered nature of P calls for additional probes to further investigate these transitions. The ANS fluorescent dye binds to hydrophobic surfaces or environments with different degrees of polarity, reflected in its maximum wavelength upon binding to the protein, and the concurrent increase in fluorescence intensity, which makes it a very sensitive complementary probe.[41] The position of the ANS fluorescence maximum depends in part on the polarity of the binding site; therefore, a more apolar binding site results in a more blue-shifted maximum wavelength. The native state of P bound ANS to a large extent, and this binding was displaced by the addition of denaturants (Figure 2B and inset). The ANS binding capacity was decreased to its baseline at 2.0 M of either denaturant, and the large fluorescence

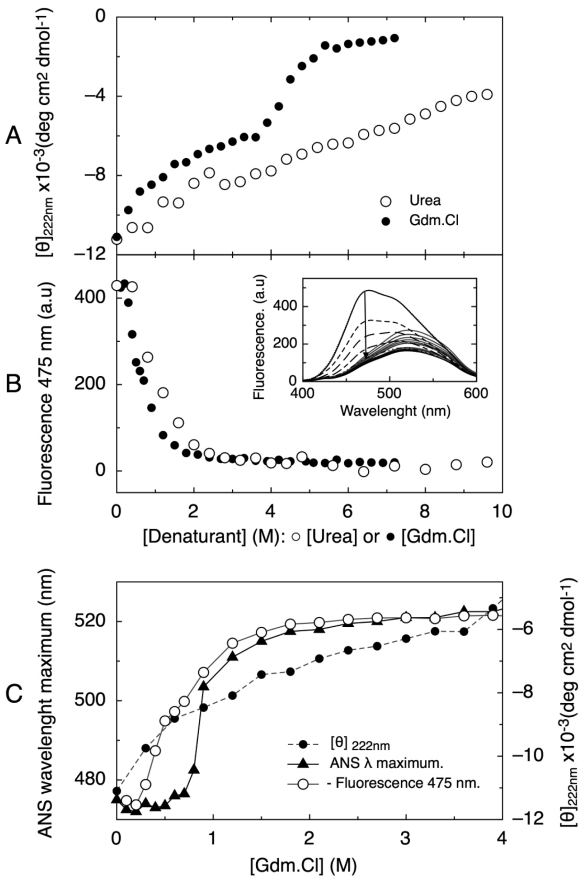

Figure 2. Conformational stability and ANS binding of P. (A) Urea (○) and Gdm.Cl (●) induced denaturation of 10 μM P monitored by changes in molar ellipticity at 222 nm. (B) Urea (○) and Gdm.Cl (●) induced denaturation of 10 μM P monitored by changes in ANS fluorescence intensity at 475 nm. The obtained fluorescence intensities were corrected for the fluorescence of free ANS in each Gdm.Cl condition. Inset: fluorescense emission spectra of 100 μM ANS and 10 μM P in increasing Gdm.Cl concentrations. The arrow indicates the decrease in fluorescence intensity at 475 nm upon the addition of increasing amounts of Gdm.Cl. (C) Uncoupling of ANS fluorescence intensity and wavelength maximum changes. Gdm.Cl induced denaturation of 10 μM P monitored by changes in molar ellipticity at 222 nm (●), inverse plot of the changes in ANS fluorescence at 475 nm (○), and changes in ANS emission maximum wavelength (▲).

intensity decrease was accompanied by a ~ 50 nm red-shift in its maximum wavelength (Figure 2C). The analysis of ANS fluorescence intensity in parallel to the wavelength maximum changes showed a clear uncoupling, which is indicative of at least two binding sites of different polarity (Figure 2C). From 0 to 0.8 M Gdm.Cl the maximum wavelength remained unchanged at a value of 475 nm, corresponding to a rather apolar environment in the native state. At that same concentration of denaturant, the ANS fluorescence intensity is already decreased by ~70% (represented as inverse in the plot). This is indicative of the presence of two types of binding events: a first, weaker and polar site with only fluorescence intensity change; a second event corresponds to the displacement of an apolar site, which approaches the maximum wavelength value of aqueous solvent exposed ANS (~520 nm). As shown in Figure 2A, there are two evident secondary structure transitions: the first matching the weak/polar

dx.doi.org/10.1021/bi300765c | Biochemistry XXXX, XXX, XXX–XXX

transition of ANS binding and the second corresponding to the complete unfolding.

Since P is a tetramer, the unfolding process must involve a dissociation event. To address this, we carried out an Gdm.Cl denaturation experiment at a lower protein concentration (1 μM), which showed a displacement of the second transition to lower denaturant concentration midpoint (Figure 3A). This

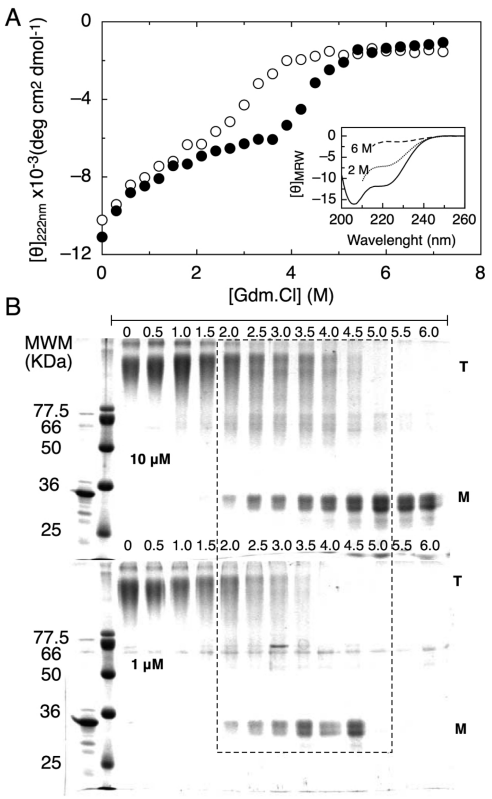

Figure 3. Concentration dependence and quaternary structure of P Gdm.Cl induced denaturation. (A) Gdm.Cl induced denaturation was followed by the molar ellipticity at 222 nm at10 μM (●) and 1 μM (○) protein concentration at 20 °C. Inset: far-UV CD spectra of native P in 20 mM sodium phosphate pH 7.4, NaCl 0.1 M (solid line) and in 2.0 and 6.0 M Gdm.Cl (indicated in the graph). (B) Quaternary structure of P as a function of Gdm.Cl concentration analyzed with glutaraldehyde cross-linking: SDS-PAGE gels showing the quaternary structure of P at two different protein concentrations (10 μM above and 1 μM below) as a function of Gdm.Cl concentration (after cross-linking with glutaraldehyde). Lane 1 displays purified P without cross-linking, lane 2 MW markers in kDa. The dashed line indicates the tetramer (T) to monomer (M) transition region, which is shifted to lower Gdm.Cl concentrations as the protein concentration decreases. In the lanes corresponding to the Gdm.Cl range 5.0–6.0 M (1 μM SDS-PAGE gel), the proteins were lost during TCA precipitation due to Gdm.Cl crystallization at high concentrations.

indicates that the first transition corresponds to an unfolding event with low cooperativity and the second steeper transition corresponds to the cooperative dissociation of the tetramer with concomitant unfolding as judged by the ellipticity change (Figure 3A). In agreement with this, the species at 2 M Gdm.Cl remained largely folded (Figure 3A, inset), and SEC experiments in 2 M Gdm.Cl at different protein concentrations indicated that it was an even more extended tetrameric species (not shown).

In order to confirm this by a different approach, we carried out chemical cross-linking along the Gdm.Cl concentration range. Each denaturant concentration point was treated with glutaraldehyde and subjected to SDS-PAGE at two different P concentrations, where only tetramers or monomers are populated (Figure 3B). As for the ellipticity monitored denaturation, there was a shift to lower denaturation midpoint at lower protein concentration, and this result allowed us to confirm the nature of the two transitions.

We produced the ~4.6 kDa Y fragment by proteolytic cleavage[31] and subjected it to chemical denaturation in order to analyze its stability and dissociation. A single transition was observed, which required less denaturant to unfold as the protein concentration was decreased, indicative of a dissociation event (Figure 4). When P and Y denaturation curves were

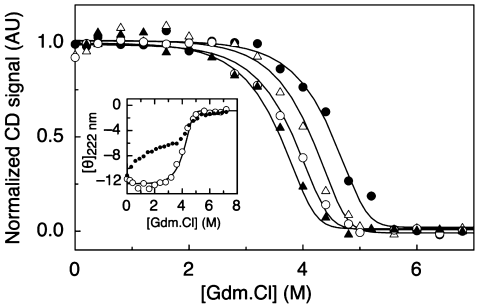

Figure 4. Concentration dependence of fragment Y Gdm.Cl induced denaturation. Gdm.Cl induced denaturation of peptide Y was followed by the molar ellipticity at 222 nm at 25.0 μM (●), 12.0 μM (△), 5.0 μM (○), and 2.5 μM (▲) concentrations at 20 °C. The CD signal at 222 nm was normalized. The data were globally fit to a two-state unfolding model (full line and see Experimental Procedures). The thermodynamic parameters estimated are $\Delta G^{H_2O} = -37.26 \pm 0.91$ kcal mol^{-1} and $m = 4.07 \pm 0.22$ kcal mol^{-1}. The inset shows the comparison of the Gdm.Cl induced denaturation of 10 μM P (●) and 12 μM fragment Y (○) monitored by molar ellipticity changes at 222 nm. The two-state model fitting of 12 μM Y denaturation is also shown as a solid line.

superimposed (Figure 4, inset), it became clear that the second unfolding transition of P corresponded to the tetramer dissociation/unfolding. The data of four denaturation curves at different peptide concentrations ranging from 2.5 to 25.0 μM were globally fitted to a tetramer−monomer unfolding equilibrium model (see Experimental Procedures). The process was characterized by a free energy of -37.26 ± 0.91 kcal mol^{-1} and m value of 4.07 ± 0.22 kcal mol^{-1} M^{-1}. This corresponds to a dissociation/unfolding constant (K_U) of 10^{-28} M^3.

Characterization of the P:M$_{2-1}$ Interaction. As mentioned in the introduction, previous pull-down experiments suggested an interaction between RSV P and the antiterminator M$_{2-1}$, both main players in the transcription/replication machinery. We wanted to address the characterization of this interaction in solution from the pure components and obtain quantitative data. We started by evaluating the physical interaction of P and M$_{2-1}$ by SEC experiments. As shown in Figure 1A, P eluted as a ~500 kDa spherical protein, whereas M$_{2-1}$ eluted as a ~100 kDa tetramer (Figure 5A). We reasoned that the disappearance of the peak corresponding to M$_{2-1}$ with the addition of increasing amounts of P would inform us of the stoichiometry of the interaction. Figure 5B shows that the gradual addition of P causes the decrease in the M$_{2-1}$ peak and a concomitant increase of the peak corresponding to the

dx.doi.org/10.1021/bi300765c | Biochemistry XXXX, XXX, XXX−XXX

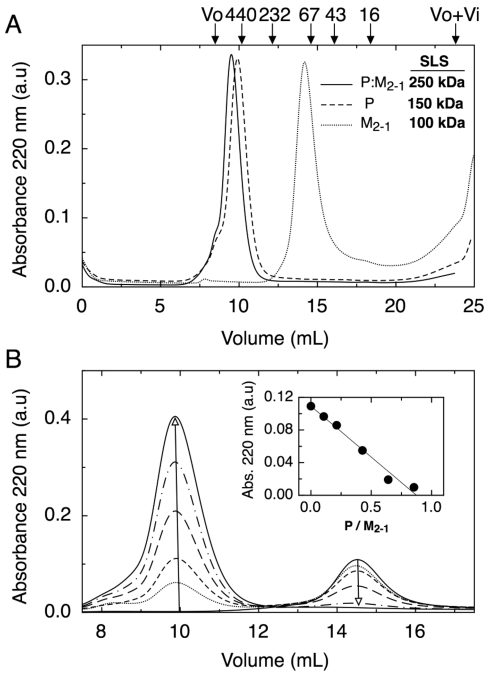

Figure 5. Hydrodynamic properties and stoichiometry of the P:M_{2-1} complex. (A) Size exclusion chromatographies of P (dashed line), M_{2-1} (dotted line), and the P:M_{2-1} complex (solid line) were carried out on a Superdex 200 HR column, equilibrated in 20 mM sodium phosphate pH 7.4, 0.3 M NaCl at 25 °C. The SLS measurements of P, M_{2-1}, and the protein complex are indicated. The stoichiometry can be derived from the total molecular weight of the complex. (B) Size exclusion chromatographies were carried out in the same conditions described above, with a fixed amount of 5 μM M_{2-1} and increasing the P protein concentration in each run as follows: 0.0, 0.5, 1.0, 2.0, 3.0, and 4.0 μM of P. The formation of the P:M_{2-1} complex (9.8 mL peak) was monitored by the absorbance decrease at 220 nm of the M_{2-1} peak (14.5 mL) upon the addition of increasing amounts of P. Inset: maximum absorbance at 220 nm of the 5 μM M_{2-1} peak as a function of the molar ratio P:M_{2-1}.

complex. The M_{2-1} peak approaches to the baseline at around a 1:1 ratio of P:M_{2-1}, establishing the actual stoichiometry obtained directly by a physical nonspectroscopic method (Figure 5B, inset). Interestingly, stoichiometric addition of P generated a 1:1 complex of the expected molecular weight (250 kDa) as determined from SLS coupled Superdex 200 SEC, which was otherwise almost superimposable with unbound P (Figure 5A). This indicated that P changes its behavior from a largely extended nonglobular molecule to a more globular conformation when bound to M_{2-1}. The use of another SEC column (Superose 6) yielded identical results (not shown).

This evident change in the hydrodynamic behavior of bound compared to unbound P led us to investigate the possible conformational changes involved. For this, we performed far-UV CD spectra of M_{2-1} alone, P alone, and the 1:1 complex mixture, and we compared the arithmetical sum of the spectra (M_{2-1} spectrum plus P spectrum) with that of the 1:1 complex mixture. The spectrum of the actual complex obtained from the mixture of the tetramers showed a substantial increase in the α-helix content (Figure 6), suggesting a structural rearrangement in one or both proteins upon the formation of the complex.

Finally, since the quantification of this interaction is essential together with the stoichiometry, we applied a fluorescence spectroscopy approach in solution. P was chemically modified with fluorescein (see Experimental Procedures), and the

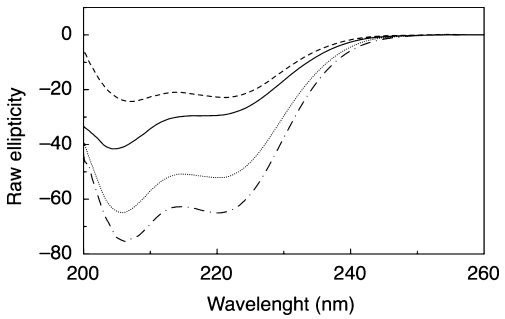

Figure 6. Structural rearrangements in the P:M_{2-1} complex determined by far UV-CD. Far UV-CD spectra of 10 μM M_{2-1} (dashed line), 10 μM P (solid line), and 10 μM of P:M_{2-1} complex (solid and dotted line) in 20 mM sodium phosphate (pH 7.4), NaCl 0.3 M, at 20 °C. The arithmetical sum of 10 μM M_{2-1} and 10 μM P spectra is also represented (dotted line).

fluorescence anisotropy value was registered upon gradual titration with M_{2-1}. The substantial anisotropy change observed reaches a plateau at a 1:1 ratio, confirming the stoichiometry obtained by SEC and suggesting a strong interaction from the shape of the titration curve (Figure 7A). We carried out titrations at lower concentrations in order to calculate a dissociation constant (Figure 7B). Experiments at 10 nM FITC-P were fitted to a simple stoichiometric binding model (see eq 1, Experimental Procedures) and obtained an average value of 8.1 ± 2.5 nM for the K_D from four independent binding curves.

DISCUSSION

The presence and role of P as an essential component of the RNA polymerase complex is a common theme in *Mononegavirales,* which include several important human pathogens. Thus, understanding its structural features, conformational stability, and interaction with other components of the polymerase complex is the basis for unraveling the molecular mechanism behind viral genome replication and transcription and a possible starting point for designing antivirals for RSV and related viruses. This is particularly so in the case of the interaction between the RSV P and M_{2-1}, polymerase cofactor, and antiterminator, respectively, which present a unique interface among the *Mononegavirales* order.

Previous work showed that P is a nonglobular homotetramer with an elongated shape, as determined by sedimentation equilibirum experiments.[31] Both P and its proteolytically cleaved tetramerization domain Y eluted from SEC as species of 4 and 3 fold their expected globular size, respectively (Figure 1A).[31] Furthermore, both His-tagged P (31.1 kDa) and fragment Y (4.9 kDa) showed an anomalous slow migration in SDS-PAGE (Figure 1B, inset), with an apparent molecular mass of 36 and 12 kDa, respectively. For other *Paramyxovirus* P proteins this was ascribed to the high content in acidic residues.[1]

Chemical denaturation of P by urea is incomplete and largely noncooperative (Figure 2A). Denaturation by Gdm.Cl leads to a three-state transition (Figures 2A and 8A) where the first one (0 to 2 M Gdm.Cl) shows little cooperativity and the second one (4 to 6 M Gdm.Cl) is a stable and cooperative transition corresponding to the dissociation/unfolding of the tetramerization domain, confirmed by the protein concentration dependence and chemical cross-linking experiments (Figure 3A,B). The first transition corresponds to actual unfolding because a

dx.doi.org/10.1021/bi300765c | *Biochemistry* XXXX, XXX, XXX−XXX

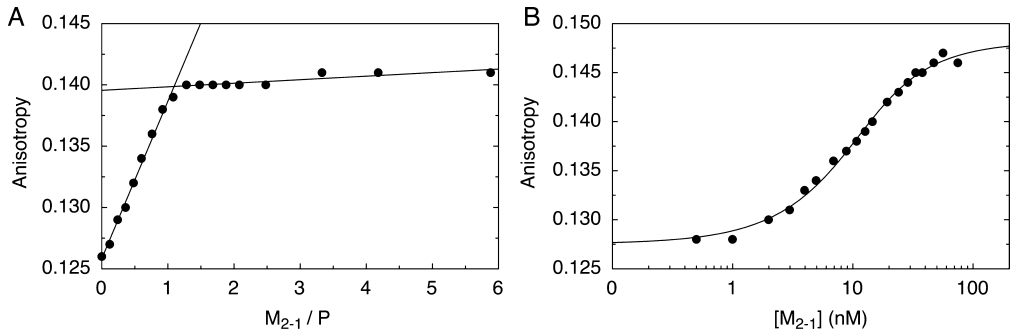

Figure 7. Fluorescence anisotropy titration of FITC labeled P with M_{2-1}. (A) Stoichiometry of the interaction: Titration of 100 nM P-FITC with increasing amounts of M_{2-1}, in 20 mM sodium phopsphate (pH 7.4), 0.3 M NaCl, 1 mM DTT, and 10 μM SO_4Zn_2, at 20 °C. The anistropy signal increased linearly up to 1:1 molar ratio, where it reached a constant value, indicating the saturation of all binding sites. (B) Titration of 10 nM P-FITC with M_{2-1} in the same conditions described above: A fit to a 1:1 binding model (see Experimental Procedures, eq 1) is shown (solid line). The binding constant obtained in this case at 20 °C was K_D = 5.2 ± 0.6 nM. Four independent binding curves at 10 nM P-FITC yielded an average K_D = 8.1 ± 2.1 nM.

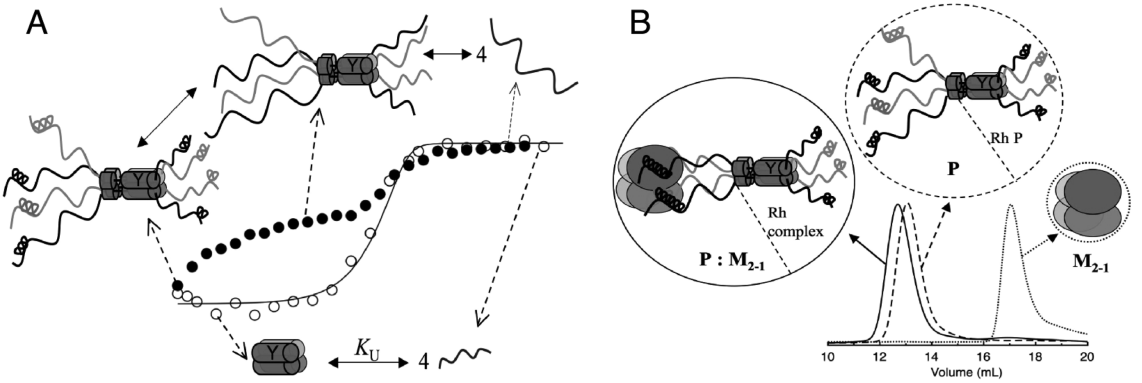

Figure 8. Model for unfolding/dissociation of RSV-P and its interaction with the antiterminator M_{2-1}. (A) Gdm.Cl induced denaturation transition states of P and the tetramerization domain Y: Gdm.Cl denaturation of P (●) leads to a three-state transition (above). The first low-cooperative unfolding transition corresponds to gradual loss of α-helical structure of either or both the N- and C-terminal domains. The second cooperative transition corresponds to dissociation−unfolding of the tetramerization domain. Gdm.Cl denaturation of fragment Y (○) leads to a two-state cooperative transition (below), between a native tetramer and an unfolded monomer. (B) Schematic representation of the P and M_{2-1} tetramers interaction: The figure shows the Superose 6 SEC elution peaks and the schematic representations of the spherical M_{2-1} tetramer; the extended P tetramer and the P:M_{2-1} complex. The hydrodynamic radii of P and the P:M_{2-1} complex are represented. Upon the formation of the complex there is a gain in the α-helix content of P and a slight increase in the hydrodynamic radius of the P:M_{2-1} complex.

substantial amount of α-helical structure is clearly lost (Figure 3A, inset). The second transition also involves the loss of α-helical structure, as expected from the 4-helix bundle configuration of the tetramerization domain, but is rather cooperative. This means that the first unfolding transition corresponds to either or both the N- and C-terminal domains (Figure 8A). Moreover, the marginal cooperativity present in the first transition indicates that, at the reference conditions, there is an equilibrium between conformations or ensembles involving α-helical structures, rather than a single, stable native conformation. The CD spectrum of P (Figure 1B) shows a shift in the typical α-helical minimum at 208 nm, which is in fact caused by the contribution of disordered (either intrinsically disordered or coil) conformations which normally present minima at around 200 nm or less.[42] Although we cannot confirm at this stage, we propose that the metastable structured domain at 20 °C is the N-terminal domain because of its larger size and because it contains the M_{2-1} binding site (see below). The noncooperative loss of transient or metastable structure suggests an intrinsically disordered nature.[43]

ANS binding experiments are very informative as they constitute a unique complementary probe for tertiary structure; they can determine the presence of hydrophobic solvent accessible sites that are present in the cores of fluctuating tertiary structures.[41] A biphasic change was observed (Figure 2B,C), which indicated two types of binding sites, one polar and solvent accessible and the other nonpolar, possibly sensing the fluctuating partly solvent accessible hydrophobic core. At 2.0 M Gdm.Cl there was no ANS binding, which is consistent with the complete unfolding of the metastable "molten globule-like" domain, leaving the highly compact and stable four-helix bundle, with no access to the hydrophobic core/tetramerization interface by the dye. Thus, the first denaturation transition corresponds to a partly folded domain with substantial secondary and possibly tertiary structure, but with marginal stability and low cooperativity. This is supported by the ability to bind ANS at a highly hydrophobic site representing a solvent accessible core, indicative of the absence of side chain packing, which results in a noncompact structure. This type of structure would also be very sensitive to proteolytic cleavage, which means that proteolysis may not only come from a disordered or instrinsically disordered structure.

The unfolding transition of the Y tetramerization domain is coincident with the second unfolding transition of P (Figure 4, inset, and Figure 8A) and allowed us to determine the overall dissociation constant of the tetramer to be 10^{-28} M^3. This

dx.doi.org/10.1021/bi300765c | Biochemistry XXXX, XXX, XXX−XXX

coiled coil arrangement is present in Ps of other *Paramyxoviruses*, and this provides the first quantitative measure for the dissociation affinity. Overall, our results indicate modularity in the RSV P protein, something that was proposed from sequence analysis but not actually determined.

Interaction between full-length P and M_{2-1} was previously determined by GST pull-down experiments[15] and using affinity chromatography with a monoclonal antibody.[14] We show that the two tetramers interact with a 1:1 stoichiometry, which is somehow unusual but explains why a discrete and soluble complex can be obtained. The interface requires a symmetrical tetrameric arrangement in both proteins. This means that if each tetramer had one interacting site per monomer, one site of each molecule (P or M_{2-1}) could interact with another site of other molecule (P or M_{2-1}). The outcome should be a network of multivalent interacting tetramers and results in oligomers or aggregates.

The hydrodynamic behavior of the P:M_{2-1} complex is almost superimposable with that of P alone. Although the complex still shows nonglobular behavior, it is smaller than the sum of the components. This is an indication of an at least partial "globularization" taking place at the complex interface (Figure 8B). The secondary structure also changes substantially upon formation of the complex, as the stoichiometric mixture of the proteins is very different from the sum of the individual spectra. The ratio 220/208 is retained, indicating that a preexisting partly folded α-helical domain is stabilized by this interaction. Altogether, these results suggest that the "globularization" and increase in α-helix are part of the same process (Figure 8B). Since the M_{2-1} binding region was mapped to the N-terminal domain of P, this structural and hydrodynamic transition upon formation of the complex must correspond to this domain. In addition, considering the hypothesis that the increase in α-helix content also corresponds to the N-terminal domain, it is tempting to suggest that the latter is the domain that undergoes the first low-cooperativity unfolding transition. This domain is noncompact, in conformational exchange at 20 °C (providing this characteristic to the full-length protein), and becomes more structured when bound to M_{2-1}. However, it appears not to be a true "intrinsically disorderded" domain.[30] This, together with unfolding results, indicate that the species after the first unfolding transition is a tetrameric true intermediate with the intact folded four-helix coiled coil, with N- and C-terminal domains in a completely unfolded conformation (Figure 8A).

The stoichiometry of the complex was confirmed using accurate fluorescence anisotropy measurements in solution (Figure 7) and determined a dissociation constant in the low nanomolar range. It was shown in this and other laboratories that RSV P as well as Ps from *Mononegavirales* members are modular proteins,[17,35] and the tetramerization domain (fragment Y) is independent of the other domains. Thus, the K_D obtained for Y represents that of the full-length P tetramer, with a value of 10^{-28} M^3. Interestingly, the K_D for the M_{2-1} tetramer shows an almost identical value of 10^{-28} M^3,[37] corresponding to a free energy of 37 kcal mol^{-1}, strongly suggesting that both proteins exist exclusively as tetramers within the cellular environment. However, we previously showed that the K_D for the M_{2-1} tetramer was drastically affected by lowering the pH within values compatible with the cell, with possible effects either or both antitermination and nucleocapsid assembly.[37,44] The range of affinity of the complex, although lower, is still rather high, and since P was shown to compete with RNA for binding to M_{2-1},[15] our results provide a clue to the range of affinity of RNA binding required for displacing the P:M_{2-1} equilibrium. However, quantitative measurements and sequence specificity, if any, remain to be established for the M_{2-1}−RNA interaction.[45]

The NMR structure for the monomeric core domain (residues 58−177) of M_{2-1} recently reported confirmed it as the P binding domain and the binding surface identified by NMR experiments.[46] A rather weak equilibrium dissociation constant of ∼3 μM was estimated for this monomeric fragment, where the reported complex was formed by one P tetramer and four M_{2-1} monomers (58−177). The picture of the interaction we now describe between the full length P and M_{2-1} consists of a tetramer−tetramer arrangement, resulting in a 1000-fold higher affinity $K_D = 8.1 \pm 2.5$ nM. Both tetramers are extremely tight, making it unlikely that they exist as monomers in the cell, and the atomic detail of the tetramer−tetramer interface remains to be established. The large difference in affinity is explained by the entropic advantage of multiple contacts between both tetramers, but changes other than those at the interface contacts should not be ruled out.

The polymerase complex components L, P, and N are present in all *Mononegavirales*, where oligomerization of P is an essential prerequisite for its activity as a cofactor of the polymerase and partake in the assembly of the complex. In this picture, dissecting the oligomerization/folding mechanism of Ps, as well as interactions with other proteins required for RNA synthesis such as M_{2-1} in the case of *Pneumoviruses*, is at the center of understanding genome replication and transcription in the *Paramyxoviridae* family.

Further investigations on the assembly mechanism of the polymerase complex from its components, including quantitative and structural analysis, will provide insights into other family members. The stability of the individual proteins and domains, its oligomerization mechanism, and the hierarchy of interactions can be successfully attained by accurate methods *in vitro*. These, in turn, will help address biochemically based questions in the context of reverse genetics and cell culture infection models of RSV, including the development of novel antivirals. In the case of RSV, the specific and unique interaction between P and M_{2-1} provides a potential target for drugs against this widespread pathogen.

AUTHOR INFORMATION

Corresponding Author

*E-mail gpg@leloir.org.ar; Ph + 54 11 5238 7500, ext. 3209; Fax + 54 11 5238 7501.

Funding

This work was supported by grant CRP/ARG10-02 from the International Centre for Biotechnology (ICGEB) and PICT-2011-0721 from ANPCyT. S.A.E., G.P., and G.P.G. are Career Investigators from Consejo Nacional de Investigaciones Científicas y Técnicas (CONICET).

Notes

The authors declare no competing financial interest.

ACKNOWLEDGMENTS

We thank Lucia Chemes and Marisol Fassolari for helpful assistance and discussions in math and fittings, Leonardo Alonso for mass spectrometry measurements, and Liliana Alonso for helpful corrections to the manuscript.

ABBREVIATIONS

RSV, respiratory syncytial virus; Gdm.Cl, guanidinium chloride; CD, circular dichroism; SEC, size exclusion chromatography; SLS, static light scattering; DLS, dynamic light scattering; IDP, intrinsically disordered proteins; ANS, 8-anilino-1-naphthalenesulfonate.

REFERENCES

(1) Kolakofsky, D., and Lamb, R. A. (2001) Paramyxoviridae. The viruses and Their replication, in *Fields Virology* (Knipe, D. M., Howley, P., Griffin, D. E., Lamb, R. A., Martin, M. A., Roizman, B., and Straus, S. E., Eds.), Lippincott Williams & Wilkins, Philadelphia.

(2) Collins, P. L., Chanock, R. M., and Murphy, B. R. (2001) Respiratory Syncytial Virus, in *Fields Virology* (Knipe, D. M., Howley, P., Griffin, D. E., Lamb, R. A., Martin, M. A., Roizman, B., and Straus, S. E., Eds.) 4th ed., Lippincott Williams & Wilkins, Philadelphia.

(3) Shay, D. K., Holman, R. C., Newman, R. D., Liu, L. L., Stout, J. W., and Anderson, L. J. (1999) Bronchiolitis-associated hospitalizations among US children, 1980−1996. *JAMA, J. Am. Med. Assoc. 282*, 1440−1446.

(4) Hall, C. B., Weinberg, G. A., Iwane, M. K., Blumkin, A. K., Edwards, K. M., Staat, M. A., Auinger, P., Griffin, M. R., Poehling, K. A., Erdman, D., Grijalva, C. G., Zhu, Y., and Szilagyi, P. (2009) The burden of respiratory syncytial virus infection in young children. *N. Engl. J. Med. 360*, 588−598.

(5) Nair, H., Nokes, D. J., Gessner, B. D., Dherani, M., Madhi, S. A., Singleton, R. J., O'Brien, K. L., Roca, A., Wright, P. F., Bruce, N., Chandran, A., Theodoratou, E., Sutanto, A., Sedyaningsih, E. R., Ngama, M., Munywoki, P. K., Kartasasmita, C., Simoes, E. A., Rudan, I., Weber, M. W., and Campbell, H. (2010) Global burden of acute lower respiratory infections due to respiratory syncytial virus in young children: a systematic review and meta-analysis. *Lancet 375*, 1545−1555.

(6) Collins, P. L., Hill, M. G., Cristina, J., and Grosfeld, H. (1996) Transcription elongation factor of respiratory syncytial virus, a nonsegmented negative-strand RNA virus. *Proc. Natl. Acad. Sci. U. S. A. 93*, 81−85.

(7) Hardy, R. W., and Wertz, G. W. (1998) The product of the respiratory syncytial virus M2 gene ORF1 enhances readthrough of intergenic junctions during viral transcription. *J. Virol. 72*, 520−526.

(8) Bermingham, A., and Collins, P. L. (1999) The M2-2 protein of human respiratory syncytial virus is a regulatory factor involved in the balance between RNA replication and transcription. *Proc. Natl. Acad. Sci. U. S. A. 96*, 11259−11264.

(9) Lamb, R. A. (2006) Mononegavirales, in *Fields Virology* (Knipe, D. M., and Howley, P., Eds.) 5th ed., pp 1357−1362, Lippincott Williams & Wilkins, Philadelphia.

(10) Garcia-Barreno, B., Delgado, T., and Melero, J. A. (1996) Identification of protein regions involved in the interaction of human respiratory syncytial virus phosphoprotein and nucleoprotein: significance for nucleocapsid assembly and formation of cytoplasmic inclusions. *J. Virol. 70*, 801−808.

(11) Castagne, N., Barbier, A., Bernard, J., Rezaei, H., Huet, J. C., Henry, C., Da Costa, B., and Eleouet, J. F. (2004) Biochemical characterization of the respiratory syncytial virus P-P and P-N protein complexes and localization of the P protein oligomerization domain. *J. Gen. Virol. 85*, 1643−1653.

(12) Tran, T. L., Castagne, N., Bhella, D., Varela, P. F., Bernard, J., Chilmonczyk, S., Berkenkamp, S., Benhamo, V., Grznarova, K., Grosclaude, J., Nespoulos, C., Rey, F. A., and Eleouet, J. F. (2007) The nine C-terminal amino acids of the respiratory syncytial virus protein P are necessary and sufficient for binding to ribonucleoprotein complexes in which six ribonucleotides are contacted per N protein protomer. *J. Gen. Virol. 88*, 196−206.

(13) Khattar, S. K., Yunus, A. S., and Samal, S. K. (2001) Mapping the domains on the phosphoprotein of bovine respiratory syncytial virus required for N-P and P-L interactions using a minigenome system. *J. Gen. Virol. 82*, 775−779.

(14) Mason, S. W., Aberg, E., Lawetz, C., DeLong, R., Whitehead, P., and Liuzzi, M. (2003) Interaction between human respiratory syncytial virus (RSV) M2−1 and P proteins is required for reconstitution of M2−1-dependent RSV minigenome activity. *J. Virol. 77*, 10670−10676.

(15) Tran, T. L., Castagne, N., Dubosclard, V., Noinville, S., Koch, E., Moudjou, M., Henry, C., Bernard, J., Yeo, R. P., and Eleouet, J. F. (2009) The respiratory syncytial virus M2−1 protein forms tetramers and interacts with RNA and P in a competitive manner. *J. Virol. 83*, 6363−6374.

(16) Fearns, R., and Collins, P. L. (1999) Role of the M2−1 transcription antitermination protein of respiratory syncytial virus in sequential transcription. *J. Virol. 73*, 5852−5864.

(17) Karlin, D., Ferron, F., Canard, B., and Longhi, S. (2003) Structural disorder and modular organization in Paramyxovirinae N and P. *J. Gen. Virol. 84*, 3239−3252.

(18) Habchi, J., and Longhi, S. (2012) Structural disorder within paramyxovirus nucleoproteins and phosphoproteins. *Mol. Biosyst. 8*, 69−81.

(19) Tarbouriech, N., Curran, J., Ruigrok, R. W., and Burmeister, W. P. (2000) Tetrameric coiled coil domain of Sendai virus phosphoprotein. *Nat. Struct. Biol. 7*, 777−781.

(20) Sanchez-Seco, M. P., Navarro, J., Martinez, R., and Villanueva, N. (1995) C-terminal phosphorylation of human respiratory syncytial virus P protein occurs mainly at serine residue 232. *J. Gen. Virol. 76* (Pt 2), 425−430.

(21) Barik, S., McLean, T., and Dupuy, L. C. (1995) Phosphorylation of Ser232 directly regulates the transcriptional activity of the P protein of human respiratory syncytial virus: phosphorylation of Ser237 may play an accessory role. *Virology 213*, 405−412.

(22) Navarro, J., Lopez-Otin, C., and Villanueva, N. (1991) Location of phosphorylated residues in human respiratory syncytial virus phosphoprotein. *J. Gen. Virol. 72* (Pt 6), 1455−1459.

(23) Mazumder, B., Adhikary, G., and Barik, S. (1994) Bacterial expression of human respiratory syncytial viral phosphoprotein P and identification of Ser237 as the site of phosphorylation by cellular casein kinase II. *Virology 205*, 93−103.

(24) Asenjo, A., Rodriguez, L., and Villanueva, N. (2005) Determination of phosphorylated residues from human respiratory syncytial virus P protein that are dynamically dephosphorylated by cellular phosphatases: a possible role for serine 54. *J. Gen. Virol. 86*, 1109−1120.

(25) Lu, B., Ma, C. H., Brazas, R., and Jin, H. (2002) The major phosphorylation sites of the respiratory syncytial virus phosphoprotein are dispensable for virus replication in vitro. *J. Virol. 76*, 10776−10784.

(26) Asenjo, A., Gonzalez-Armas, J. C., and Villanueva, N. (2008) Phosphorylation of human respiratory syncytial virus P protein at serine 54 regulates viral uncoating. *Virology 380*, 26−33.

(27) Asenjo, A., Calvo, E., and Villanueva, N. (2006) Phosphorylation of human respiratory syncytial virus P protein at threonine 108 controls its interaction with the M2−1 protein in the viral RNA polymerase complex. *J. Gen. Virol. 87*, 3637−3642.

(28) Mazumder, B., and Barik, S. (1994) Requirement of casein kinase II-mediated phosphorylation for the transcriptional activity of human respiratory syncytial viral phosphoprotein P: transdominant negative phenotype of phosphorylation-defective P mutants. *Virology 205*, 104−111.

(29) Asenjo, A., and Villanueva, N. (2000) Regulated but not constitutive human respiratory syncytial virus (HRSV) P protein phosphorylation is essential for oligomerization. *FEBS Lett. 467*, 279−284.

(30) Llorente, M. T., Garcia-Barreno, B., Calero, M., Camafeita, E., Lopez, J. A., Longhi, S., Ferron, F., Varela, P. F., and Melero, J. A. (2006) Structural analysis of the human respiratory syncytial virus phosphoprotein: characterization of an alpha-helical domain involved in oligomerization. *J. Gen. Virol. 87*, 159−169.

(31) Llorente, M. T., Taylor, I. A., Lopez-Vinas, E., Gomez-Puertas, P., Calder, L. J., Garcia-Barreno, B., and Melero, J. A. (2008) Structural properties of the human respiratory syncytial virus P protein: evidence

882 for an elongated homotetrameric molecule that is the smallest
883 orthologue within the family of paramyxovirus polymerase cofactors.
884 *Proteins 72*, 946−958.
885 (32) Tarbouriech, N., Curran, J., Ebel, C., Ruigrok, R. W., and
886 Burmeister, W. P. (2000) On the domain structure and the
887 polymerization state of the sendai virus P protein. *Virology 266*, 99−
888 109.
889 (33) Rahaman, A., Srinivasan, N., Shamala, N., and Shaila, M. S.
890 (2004) Phosphoprotein of the rinderpest virus forms a tetramer
891 through a coiled coil region important for biological function. A
892 structural insight. *J. Biol. Chem. 279*, 23606−23614.
893 (34) Poh, S. L., el Khadali, F., Berrier, C., Lurz, R., Melki, R., and
894 Tavares, P. (2008) Oligomerization of the SPP1 scaffolding protein. *J.*
895 *Mol. Biol. 378*, 551−564.
896 (35) Gerard, F. C., Ribeiro Ede, A., Jr., Leyrat, C., Ivanov, I., Blondel,
897 D., Longhi, S., Ruigrok, R. W., and Jamin, M. (2009) Modular
898 organization of rabies virus phosphoprotein. *J. Mol. Biol. 388*, 978−
899 996.
900 (36) Hermanson, G. T. (1996) *Bioconjugate Techniques*, Academic
901 Press, San Diego, CA.
902 (37) Esperante, S. A., Chemes, L. B., Sanchez, I. E., and de Prat-Gay,
903 G. (2011) The respiratory syncytial virus transcription antiterminator
904 M(2−1) is a highly stable, zinc binding tetramer with strong pH-
905 dependent dissociation and a monomeric unfolding intermediate.
906 *Biochemistry 50*, 8529−8539.
907 (38) Smal, C., Wetzler, D. E., Dantur, K. I., Chemes, L. B., Garcia-
908 Alai, M. M., Dellarole, M., Alonso, L. G., Gaston, K., and de Prat-Gay,
909 G. (2009) The human papillomavirus E7-E2 interaction mechanism in
910 vitro reveals a finely tuned system for modulating available E7 and E2
911 proteins. *Biochemistry 48*, 11939−11949.
912 (39) Mateu, M. G., and Fersht, A. R. (1998) Nine hydrophobic side
913 chains are key determinants of the thermodynamic stability and
914 oligomerization status of tumour suppressor p53 tetramerization
915 domain. *EMBO J. 17*, 2748−2758.
916 (40) Uversky, V. N. (2002) Natively unfolded proteins: a point
917 where biology waits for physics. *Protein Sci. 11*, 739−756.
918 (41) Slavik, J. (1982) Anilinonaphthalene sulfonate as a probe of
919 membrane composition and function. *Biochim. Biophys. Acta 694*, 1−
920 25.
921 (42) Fasman, G. D., Ed. (1996) *Circular Dichroism and the*
922 *Conformational Analysis of Biomolecules*, Plenum Press, New York.
923 (43) Uversky, V. N. (2009) Intrinsically disordered proteins and their
924 environment: effects of strong denaturants, temperature, pH, counter
925 ions, membranes, binding partners, osmolytes, and macromolecular
926 crowding. *Protein J. 28*, 305−325.
927 (44) Li, D., Jans, D. A., Bardin, P. G., Meanger, J., Mills, J., and
928 Ghildyal, R. (2008) Association of respiratory syncytial virus M
929 protein with viral nucleocapsids is mediated by the M2−1 protein. *J.*
930 *Virol. 82*, 8863−8870.
931 (45) Cuesta, I., Geng, X., Asenjo, A., and Villanueva, N. (2000)
932 Structural phosphoprotein M2−1 of the human respiratory syncytial
933 virus is an RNA binding protein. *J. Virol. 74*, 9858−9867.
934 (46) Blondot, M.-L., Dubosclard, V., Fix, J., Lassoued, S., Aumont-
935 Nicaise, M., Bontems, F., Eléouët, J.-F., and Sizun, C. (2012) Structure
936 and Functional Analysis of the RNA- and Viral Phosphoprotein-
937 Binding Domain of Respiratory Syncytial Virus M2−1 Protein. *PLOS*
938 *Pathog.*, 8.